JACS
JOURNAL OF THE AMERICAN CHEMICAL SOCIETY

Article

pubs.acs.org/JACS

An Electrochemical Quartz Crystal Microbalance Study of a Prospective Alkaline Anion Exchange Membrane Material for Fuel Cells: Anion Exchange Dynamics and Membrane Swelling

Jimmy John, Kristina M. Hugar, Johary Rivera-Meléndez, Henry A. Kostalik, IV, Eric D. Rus, Hongsen Wang, Geoffrey W. Coates, and Héctor D. Abruña*

Department of Chemistry and Chemical Biology, Baker Laboratory, Cornell University, Ithaca, New York 14853-1301, United States

Supporting Information

ABSTRACT: A strategy has been devised to study the incorporation and exchange of anions in a candidate alkaline anion exchange membrane (AAEM) material for alkaline fuel cells using the electrochemical quartz crystal microbalance (EQCM) technique. It involves the electro-oxidation of methanol (CH_3OH) under alkaline conditions to generate carbonate (CO_3^{2-}) and formate ($HCOO^-$) ions at the electrode of a quartz crystal resonator coated with an AAEM film, while simultaneously monitoring changes in the frequency (Δf) and the motional resistance (ΔR_m) of the resonator. A decrease in Δf, indicating an apparent mass increase in the film, and a decrease in ΔR_m, signifying a deswelling of the film, were observed during methanol oxidation. A series of additional QCM experiments, in which the effects of CH_3OH, CO_3^{2-}, and $HCOO^-$ were individually examined by changing the solution concentration of these species, confirmed the changes to be due to the incorporation of electrogenerated $CO_3^{2-}/HCOO^-$ into the film. Furthermore, the AAEM films were found to have finite anion uptake, validating the expected tolerance of the material to salt precipitation in the AAEM. The EQCM results obtained indicated that $HCOO^-$ and CO_3^{2-}, in particular, interact strongly with the AAEM film and readily displace OH^- from the film. Notwithstanding, the anion exchange between $CO_3^{2-}/HCOO^-$ and OH^- was found to be reversible. It is also inferred that the film exhibits increased swelling in the OH^- form versus the $CO_3^{2-}/HCOO^-$ form. Acoustic impedance analysis of the AAEM-film coated quartz resonators immersed in water showed that the hydrated AAEM material exhibits significant viscoelastic effects due to solvent plasticization.

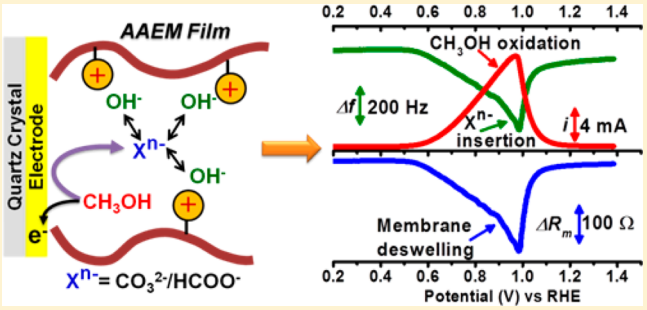

1. INTRODUCTION

Low temperature fuel cells (operating at <100 °C) are attractive as energy conversion devices for electric vehicles as well as for powering portable devices. They have been specifically targeted for deployment in electric vehicles because of their high specific energy density, which is comparable to that of internal combustion engines (ICEs).[1] Compared to other transportation electrification schemes based on batteries and supercapacitors, fuel cells afford the operational ease of the current ICE-powered cars in terms of (1) fast recharging (refueling) times (<5 min) and (2) enhanced range (~300 mi).[2] Among the low temperature fuel cells, proton exchange membrane fuel cells (PEMFCs) have evolved into a mature technology over the last 50 years, mainly due to the successful application and optimization of Nafion as the PEM.[3] However, the efforts at finding efficient, stable, and inexpensive electrocatalysts that can replace those based on platinum group metals (PGM) have not been successful. The acidic operating conditions of PEMFCs seem to fundamentally preclude the use of less noble, inexpensive metals as electrocatalysts in PEMFCs, especially for the oxygen reduction reaction (ORR).

Alkaline fuel cells (AFCs) could provide a potential cost advantage since many of the candidate non-PGM electrocatalyst materials are stable under alkaline operating conditions.[4−6] Even for Pt-based electrocatalysts, the alkaline operation is expected to be beneficial since it endows higher tolerance to CO, a common poisoning species, on Pt vis-à-vis acidic medium.[7,8] Historically, AFCs were the first to be deployed on an industrial scale for energy generation in the Apollo series of space missions using on-board H_2 and O_2 supplies.[9] However, their terrestrial usage was problematic because of the issue of carbonate salt precipitation (vide infra).

Traditionally, AFCs were based on the use of liquid electrolytes. A saturated KOH solution contained in a porous matrix (such as asbestos) served as the electrolyte medium. Trace amounts of CO_2 in the reactant feed streams would be converted to CO_3^{2-} (a process known as carbonation) at the

Received: November 18, 2013
Published: March 3, 2014

   dx.doi.org/10.1021/ja4117457 | J. Am. Chem. Soc. 2014, 136, 5309−5322

basic operating pH (as per eq 1) in such systems. Over time, CO_3^{2-} would accumulate in the electrolyte, combining with the

$$CO_{2(aq)} + 2OH^-_{(aq)} \rightarrow CO^{2-}_{3(aq)} + H_2O \quad (1)$$

potassium (K^+) cations, to eventually precipitate out as the salt K_2CO_3 (eq 2). This process deleteriously affects the performance of the fuel cell. First, since the formation of CO_3^{2-} consumes OH^- (eq 1), the conductivity of the electrolyte is lowered.[10,11] Second, the precipitate can coat electrodes and gas diffusion layers restricting the accessibility of reactants to the electrode surfaces.[4,10−12] Furthermore, the salt deposits in the electrolyte can grow to such an extent that they obstruct the free transport of OH^- from the cathode to the anode through the porous matrix. To circumvent this issue, recirculation of the liquid-electrolyte and the removal of CO_2 in the incoming gases by the use of CO_2 scrubbers was employed with some success, of course, at the expense of increased operational complexity.[10]

$$2K^+_{(aq)} + CO^{2-}_{3(aq)} \rightarrow K_2CO_{3(s)}\downarrow \quad (2)$$

In principle, the replacement of the liquid electrolyte by a solid polymer electrolyte (SPE)/ionomer, analogous to the PEM in PEMFCs, could address the problem of carbonate precipitation. It is to be noted that, in traditional AFCs, the precipitation of the carbonate salt is the combined effect of the significantly lower solubility of K_2CO_3 (vis-à-vis KOH)[13] and the excess availability of free K^+ ions. However, in a OH^- conducting SPE, the cations are covalently immobilized and spatially separated on a polymer backbone. Consequently, although CO_3^{2-} ions could pair with the cations, the precipitation of the salt itself should be precluded.[4,10] Recently, there has been a surge in the development of such cationic OH^- conducting SPEs known as alkaline anion exchange membranes (AAEMs).[11,12,14] This has, in turn, initiated a resurgence in the study of the AFCs, now based on the use of AAEMs as the electrolyte.[4] At this point, it should be mentioned that there are different types of AAEMs, such as homogeneous membranes, heterogeneous membranes, and interpenetrating polymer networks.[11,12,14] Of these, the homogeneous membranes, which are macroscopically single phase materials, are the most promising as they do not require the addition of KOH (or base) solution to bestow ionic conductivity on the membranes. In the present work, AAEMs are taken to refer to this type of materials.

Chemically, AAEMs are copolymers that consist of structural (hydrophobic) and functional (hydrophilic and cationic) segments. The functional units are typically quaternary heterocations such as those of nitrogen (N) or phosphorus (P) covalently tethered to a hydrophobic polymer backbone. Recent comprehensive reviews can be referred to for an exhaustive treatment of the AAEM materials investigated so far.[11,12,14] There are critical issues to be addressed before AAEMs can be widely deployed in AFCs. On the materials side, the key challenges are improving the chemical/base stability of the membranes at high operating pH and temperatures, achieving high OH^- conductivity in the membrane and development of soluble forms of the AAEMs for use in the fabrication of membrane-electrode assemblies (MEAs) for devices.[4] Over the past few years, our contributions to AAEM research includes the development of materials that are highly base stable,[15] that exhibit high OH^- conductivity,[16] and that are solvent-processable.[17]

Despite the considerable progress made in the field of AAEMs in a short span of time, a fundamental knowledgebase of the critical membrane processes still needs to be pursued by extensive analytical studies. The mechanism of charge transport, in general, and OH^- transport, in particular, in the membranes,[18,19] the effect of carbonation on the membranes,[20] and the influence of polymer morphology/microstructure on the membrane properties[21] represent some important avenues for further fundamental investigations in the field. In line with this research direction, in the present work, we sought to investigate the process of anion incorporation, in general, and carbonate uptake, in particular, in AAEMs. To this end, we chose to study the anion exchange dynamics in a prospective AAEM material[17] previously developed by us (Figure 1a). An additional focus of the present work is the solvent swelling of AAEMs. AAEMs need to be sufficiently hydrated to exhibit ionic conductivity. However, at the same time, AAEMs undergo swelling on hydration, and excessive swelling will result in a loss of the mechanical integrity of the membrane.[21] Hence, it is important to look at the effects of water-uptake on AAEMs. To this end, in addition to the anion exchange studies, we also investigated the changes in the swelling of the membrane on its hydration and also in situ during the anion exchange process.

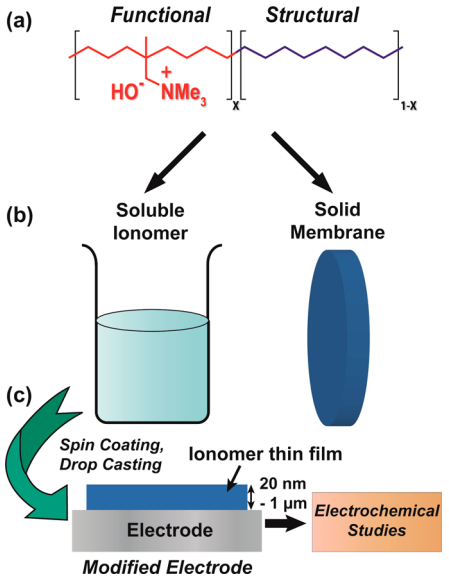

Figure 1. (a) Chemical structure of the AAEM studied. (b) Solvent processability of the AAEM material. (c) Preparation of ionomer-film modified electrodes from the ionomer solution.

The candidate material (Figure 1a), which is the subject of the present work, consists of a polyethylene backbone (structural unit) with a quaternary-ammonium cation (functional unit) tethered to the backbone by an alkyl side chain. Because of its chemical simplicity, the material can be considered a prototypical AAEM. The ex situ characterization of the material demonstrated the membranes to be mechanically stable and to exhibit fairly high OH^- conductivity (44 mS/cm at 20 °C).[17] Significantly, this material is also solvent processable; i.e., depending on the choice of solvents, the polymer can be either cast as the solid membrane or dissolved in a suitable solvent to yield ionomer solutions (Figure 1b). This property allows the material to be used in

dx.doi.org/10.1021/ja4117457 | J. Am. Chem. Soc. 2014, 136, 5309−5322

catalyst-ionomer inks for fuel cell membrane electrode assembly (MEA) preparation. The availability of the soluble ionomer form also enabled the electroanalytical studies of the material, reported herein, as thin films of the material can be formed on an electrode substrate by spin-coating from the ionomer solution (Figure 1c).

2. METHODOLOGY

2.1. Electrochemical Quartz Crystal Microbalance. In the quartz crystal microbalance (QCM) technique, oscillating quartz crystals act as mass sensors for monitoring processes that involve addition or removal of material. The technique is highly versatile since the crystals can be operated in widely different environments ranging from vacuum to liquids. In short, the QCM employs a quartz crystal oscillating at a particular resonant frequency, and the deposition of mass (Δm) on the crystal causes a decrease in the resonant frequency, and vice versa. The resulting frequency change (Δf) can be measured with high precision and related to the mass change (Δm); thus, the oscillating quartz crystal acts as a mass sensor. The electrochemical-QCM (EQCM) technique is an extension of the QCM technique in which a quartz crystal, integrated into an electrochemical setup, is used to detect mass changes at the electrode surface accompanying electrochemical processes. For a comprehensive treatment of the EQCM technique, the highly readable review by Buttry and Ward can be referred to.[22]

In the present work, we have employed the EQCM technique to study the incorporation and exchange of anions such as CO_3^{2-} and $HCOO^-$ in ionomer thin films deposited on top of the quartz crystal electrodes. The strategies utilized are depicted in Figure 2 . The first

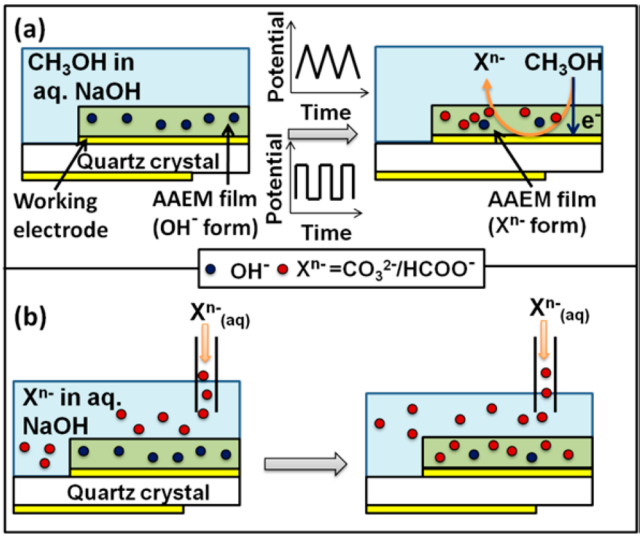

Figure 2. Depiction of the two strategies to study anion exchange dynamics in AAEM thin films using EQCM technique. (a) Local generation of anions, X^{n-} (= CO_3^{2-}/$HCOO^-$), electrochemically by oxidation of a carbonaceous fuel (CH_3OH) at the AAEM-film modified electrode. (b) Ion-exchange of OH^- in the film by X^{n-} in the solution by the addition of aliquots of $X^{n-}_{(aq)}$ to the solution at open circuit.

method (Figure 2a) consisted of electrochemically generating anions, X^{n-} (= CO_3^{2-}/$HCOO^-$), through the oxidation of a carbonaceous fuel, such as CH_3OH, at the ionomer-film modified QCM electrode. In this way, the exchange of OH^- by the locally generated X^{n-} in the film can be monitored by measuring the changes in the crystal frequency (Δf). It should be noted that in this method, the solution concentration of the various species remains unchanged.

A complementary strategy in which aliquots of X^{n-}(aq) were added to the solution with the cell at open circuit, i.e., in the absence of any potential control, and simultaneously monitoring Δf is depicted in Figure 2b. This allows deconvolution of the individual contributions of the various species involved in the ion-exchange process in the ionomer film. In this case, unlike the previous method, the displacement of OH^- from the film is driven by the increasing bulk solution concentration of X^{n-}.

2.2. Acoustic Impedance Analysis. An oscillating quartz crystal responds not only to mass changes at the crystal, but also to the changes in the rheology of its surrounding medium. Consider a typical scenario of operation of the quartz crystal in EQCM experiments where there is mass loading on the crystal in the form of a film, and the crystal itself is immersed in a liquid medium (Figure 3a). Since the

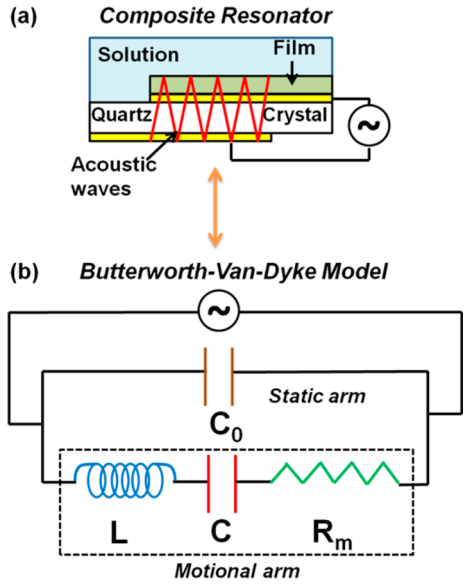

Figure 3. (a) An oscillating mass-loaded quartz crystal immersed in a liquid medium acting as a composite resonator. (b) The corresponding equivalent electrical circuit as per the Butterworth–Van-Dyke Model.

acoustic waves produced by the oscillating crystal span both the crystal and the deposited film, the film-modified quartz crystal is said to act as a composite resonator which, in turn, is affected by the liquid medium in which it is immersed. The operation of the composite resonator in such a situation can be generally modeled by equivalent electrical circuits, of which the most commonly used is the Butterworth–Van-Dyke (BVD) model (Figure 3b).[22]

The utility of the electrical equivalent models lies in the fact that each of the circuit elements represents a phenomenological aspect of the operation of the composite resonator, and the corresponding circuit parameter, as per the applied model, can be determined experimentally by acoustic impedance spectroscopy. It is beyond the scope of this manuscript to review the theory of acoustic impedance analysis. The review by Buttry and Ward offers an accessible introduction to the subject.[22]

For the sake of the subsequent discussion of the results, the salient points of the BVD model are summarized here. The BVD model consists of a series LCR circuit known as the motional arm, in parallel with a capacitor of capacitance C_0. The motional arm models the behavior of the composite resonator as a damped harmonic oscillator. The inductance L, the capacitance C, and the resistance R_m (known as the motional resistance) are related to the mass loading, the elasticity and the dissipation losses of the composite resonator, respectively. Specifically, increases in the experimentally determined values of L, C, and R_m will correspond to an increase in the mass loading, a decrease in the "stiffness", and an increase in the dissipation loss of the composite resonator, respectively. This analysis is invaluable since it readily diagnoses any nonideality of the film deposited such as viscoelastic losses that indicate its non/semirigid behavior. For a realistic model of the composite resonator, a capacitance C_0 is included

dx.doi.org/10.1021/ja4117457 | J. Am. Chem. Soc. 2014, 136, 5309–5322

(known as the static arm), parallel to the motional arm, to account for the static capacitance of the quartz crystal with the electrodes.[22]

3. EXPERIMENTAL SECTION

3.1. Preparation of Ionomer-Film Modified QCM Electrodes. The polymer was synthesized following the procedures that we reported previously.[17] All samples were prepared with a 1:3.75 molar ratio of functional to nonfunctional (structural) units (x = 0.21 in Figure 1a). This ratio afforded the best combination of mechanical stability and ionic conductivity. The polymer samples were synthesized in the iodide (I^-) form. Since I^- can strongly adsorb on metal surfaces, such as the Pt electrodes of the QCM, the I^- in the samples was exchanged first with OH^- and then finally with CO_3^{2-} following the procedure outlined below.

The samples in the I^- form were first immersed in 1 M base (NaOH or KOH) for 20 min with stirring. The step was repeated with a fresh aliquot of base solution to ensure that all the I^- was exchanged with OH^-. The sample in the OH^- form was subsequently immersed in 1 M Na_2CO_3, and the ion-exchange carried out as previously. Finally, any excess base or carbonate was removed by soaking in deionized (DI) water with stirring for 20 min. This process was repeated twice with a fresh batch of DI water each time. The dried CO_3^{2-} exchanged material is air stable and can be stored and subsequently used to make ionomer solutions.

The wet polymer sample in the CO_3^{2-} form, obtained after the ion-exchange procedure, was dried between sheets of tissue to remove most of the water. The sample was further dried overnight at room temperature by placing in a partially evacuated chamber. The dried sample was then weighed. On the basis of the measured weight and the desired wt % of the polymer in the final ionomer solution, an appropriate volume of *n*-propanol was added to the dried sample in a glass vial with a stir bar. The capped vial was then placed in a silicone oil bath on a magnetic stirrer with an automatic temperature feedback control (IKA Works Ceramag Midi with ETS-D4 temperature monitor). Typically, the temperature of the bath was set to ∼80 °C. The solution was left stirring at the elevated temperature for at least 24 h to ensure complete dissolution.

The spin-coating of ionomer thin films on the quartz crystals was performed using a commercial spin-coater (Laurell Model WS-400A-6NPP/LITE). The quartz crystals were cleaned initially in a Chromerge bath. They were then washed with *n*-propanol and deionized (DI) water and blow-dried using a jet of dry air/argon. The crystals were then mounted and secured on the chuck of the spin-coater. An aliquot of the ionomer solution, which was sonicated for 10−15 min beforehand, was then introduced onto the stationary substrate using a micropipet. Immediately afterward, the spin-coater program was initiated. The spin-coater was ramped up to its final speed where it was left for an appropriate amount of time so as to remove any residual solvent. The resulting film was then dried in a slow jet of dry air/argon.

It is to be noted that the ionomer films used for all the measurements, both acoustic impedance and EQCM, were always prepared in the CO_3^{2-} form following the ion-exchange procedure outlined previously. This protocol was followed, as the dry films are chemically more stable in the CO_3^{2-} form than in the OH^- form. For the EQCM experiments, there was always a stabilization period of about 3−4 h where the crystal frequency was allowed to reach a steady-state behavior before the actual experiment was initiated. Since the film was kept immersed in stirred NaOH solution during this stabilization period, the CO_3^{2-} ions were exchanged out for the OH^- ions in solution. Hence, for the EQCM studies, the films were in the OH^- form at the start of the experiments.

3.2. Film Thickness Measurement. The dry thicknesses of the spin-coated ionomer films on the quartz electrode substrates were measured by a contact profilometer (Tencor Alpha Step 500). Films were always deposited on a pair of similar substrates, and identical conditions of spin-coating were employed on both. One of the samples was used for profilometry and the other sample was used for electrochemical experiments. The thicknesses of both film samples prepared under identical conditions were assumed to be the same.

For profilometry, step edges were created in the film using a pointed cotton or foam head swab lightly soaked in *n*-propanol. Line scans were performed across at different points along the edges. The thickness readings were then averaged to determine the mean film thickness. The film thicknesses reported in the current study are always for the dry film.

3.3. EQCM Apparatus. 5 MHz AT-cut quartz crystals with polished Au or Pt electrode surfaces were purchased from Maxtek, Inficon, Tangidyne and Stanford Research Systems (SRS). The quartz crystals were 1″ in diameter with the electrodes arranged in the asymmetric keyhole configuration. The diameter of the front electrode (solution side) of the quartz crystal was ca. 0.5″ (geometric area = 1.37 cm^2), and the back electrode was ca. 0.25″ in diameter (geometric area = 0.32 cm^2). In case of $HCOO^-$ oxidation (discussed later), a Pd thin film (∼100 nm thick) was deposited by Ar-sputtering on top of the Au electrode of a quartz crystal.

An SRS EQCM setup was employed to operate the quartz crystal and collect the frequency (f) and the motional resistance (R_m) values during the course of the electrochemical experiments. The quartz crystals were mounted in a Teflon holder (SRS Model No. O100RH) and driven by an oscillator circuit housed in an external electronics module (SRS Model No. O100RXO). This module also realizes the galvanic isolation of the QCM measurements from the electrochemical measurements and allows for the working-electrode lead of the potentiostat to be connected to the front face (the working electrode) of the crystal. The f and the R_m values of the crystal were measured by a controller unit (SRS Model QCM 200), which outputs the data via a serial cable to a computer where they were read by a SRS LabVIEW program (SRS QCM 200).

A standard three-electrode configuration was employed for the electrochemistry segment of the EQCM experiments with the front electrode of the quartz crystal acting as the working electrode. A reversible hydrogen electrode (RHE) or a Ag/AgCl electrode was used as the reference electrode. However, the potentials are always referenced to the RHE scale for all results presented in this manuscript. A large area Pt-wire coil was used as the counter electrode. A water-jacketed glass cell, equipped with a custom-made Teflon lid, was employed. Besides having the provision to hold the electrodes in place inside the cell, the Teflon lid also had ports that allowed gases and/or solutions to be introduced into the cell. Since the crystal operation is sensitive to local variations in temperature, the solution inside the cell was maintained at a constant temperature (25 °C) by means of a thermostat (Fischer Scientific Model No. 9101), which circulated water through the jacket surrounding the cell. In order to mitigate any frequency drifts due to random convection currents in the solution, the solution was stirred using a stir-bar that was operated by a magnet driven by a jet of compressed air. The potentiostats employed for the experiments were a Pine AFCBPI Bipotentiostat and a BASi CV-27 voltammograph. The data from the potentiostats were recorded using a homemade LabVIEW program via a NI-DAQ card.

3.4. Acoustic Impedance Spectroscopy. The acoustic impedance responses of the composite resonators were obtained using a Hewlett-Packard impedance analyzer (Model No. HP4194A). The crystal mounted in the SRS holder was connected to the analyzer via a 16047D test fixture (Hewlett-Packard). It should be pointed out that the SRS crystal holder does not include the oscillator circuit. This allows the impedance analyzer to drive the crystal at off-resonant frequencies. The data were recorded by an HP developed LabVIEW program through a GPIB interface.

3.5. Chemicals. Methanol (anhydrous AR ACS Macron chemicals), sodium carbonate (100.0% AR ACS Mallinckrodt) and sodium formate (≥99.0% puriss p.a. ACS Sigma Aldrich) were used for the studies. Additionally, for ion-exchange procedures and for making supporting electrolyte solutions, sodium hydroxide (98.7% AR ACS Macron chemicals) was employed. Solutions were prepared in high purity deionized water (18 MΩ cm Barnstead Nanopure Model No. 7148). For deaerating the solutions and maintaining an inert

dx.doi.org/10.1021/ja4117457 | J. Am. Chem. Soc. 2014, 136, 5309−5322

atmosphere in the EQCM cell, high purity nitrogen and argon gases were obtained from Airgas.

4. RESULTS AND DISCUSSION

4.1. Acoustic Impedance Analysis. The motivation for performing the acoustic impedance spectroscopy of the ionomer-film modified quartz crystal electrodes is 2-fold. First, since it is known that the AAEM material swells on hydration,[17] the validity of the rigid film behavior of the ionomer film during the operation of the crystal was suspect and needed to be verified. This was important for mass quantification since the linear relationship between the frequency change (Δf) and the mass change (Δm) at the quartz crystal, as given by the Sauerbrey equation (eq 3), is valid only for uniform, rigid thin films.[22]

$$\Delta f = -C_f \Delta m \tag{3}$$

In this equation C_f is the sensitivity factor. Second, the results from the impedance analysis guided the choice of ionomer thin film parameters (such as the thickness) for the EQCM studies (vide infra).

In the impedance analysis of a composite resonator, the impedance (Z) or its inverse, admittance ($Y = 1/Z$), is measured over a frequency range spanning the frequencies $f_{|Z|_{min}}$ and $f_{|Z|_{max}}$ at which the magnitude of the impedance, $|Z|$, is at the minimum and the maximum values, respectively. Y and Z being complex quantities, they can be cast either in the polar or the rectangular form as shown below in eqs 4 and 5, respectively.

$$Z = |Z|e^{i\theta} = R + iX \tag{4}$$

$$Y = G + iB \tag{5}$$

where θ, R, X, G, B are the phase angle, the resistance, the reactance, the conductance and the susceptance of the entire impedance network representing the composite resonator.

For composite resonators that can achieve resonance (vide infra), $f_{|Z|_{min}}$ and $f_{|Z|_{max}}$ are the same as the series (f_s) and the parallel (f_p) resonant frequencies respectively. Referring to the BVD model (Figure 3b), the series resonance occurs when the reactances of the motional arm components cancel out. The parallel resonance happens at a higher frequency when the susceptances of the motional and the static arm cancel each other out.

For diagnosing viscoelastic effects in a composite resonator, typically, $|Z|-\theta$, $G-B$, and admittance locus (B vs G) plots are constructed and analyzed.[22] Viscoelastic effects refer to the non/semirigid behavior of a deposited film on the quartz crystal. The effects are termed viscoelastic because the film introduces a viscous loading (like a liquid) due to its non/semirigidity while, at the same time, still retaining some amount of elastic behavior characteristic of a rigid solid film. For the current discussion, the plots of θ and G versus frequency (f) and the admittance locus are utilized to highlight the viscoelastic effects introduced by the hydrated ionomer thin film on the operation of the quartz crystal. To this end, the acoustic impedance data were collected and analyzed for a series of ionomer thin films of varying thickness, deposited on the quartz crystal, in both the dry and the hydrated state. For the theoretical framework needed for the interpretation of the impedance plots, the readers are referred to the literature available elsewhere.[22]

In constructing plots of θ and G vs f, we have opted to make use of relative frequencies (Δf) as defined below in lieu of the absolute frequencies (f). For θ-plots, $\Delta f = f - (f_{|Z|_{min}} + f_{|Z|_{max}})/2$ and for G-plots, $\Delta f = f - f_{G_{max}}$, where $f_{G_{max}}$ is the absolute frequency at which G is maximum. The use of Δf, in the manner outlined above, compensates for the shifts in the resonant frequencies of the composite resonators due to (1) the sample variations in the bare QCM electrodes used to prepare the film-modified electrodes and (2) the mass loading of the crystal by the ionomer film. This allows for a direct qualitative comparison of the impedance responses of the series of ionomer-film modified QCM electrodes with different film thicknesses.

By comparing the θ-response of the hydrated ionomer-film modified QCM electrode in water (Figure 4a) to that of the dry

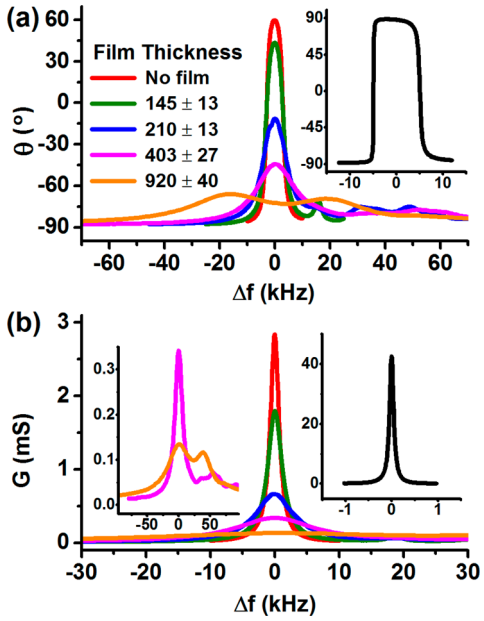

Figure 4. (a) θ vs Δf plots for a series of ionomer films (in the CO_3^{2-} form) of different dry thicknesses on Pt QCM electrodes at room temperature (~21 °C) in deionized water. The inset shows the corresponding θ vs Δf plot for the 920 nm thick dry ionomer-film modified QCM electrode in air. (b) The corresponding G vs Δf series of plots for the same set of ionomer-film modified QCM electrodes in deionized water as in (a). The legend of (a) is applicable to (b). The right-hand-side inset shows the corresponding G vs Δf plot for the 920 nm thick dry ionomer-film modified QCM electrode in air. The left-hand-side inset shows the expanded conductance plots for the 403 and the 920 nm film-modified QCM electrodes in water. $\Delta f = f - (f_{|Z|_{min}} + f_{|Z|_{max}})/2$ for (a) and $\Delta f = f - f_{G_{max}}$ for (b), where f is the absolute frequency, and $f_{|Z|_{min}}$, $f_{|Z|_{max}}$, and $f_{G_{max}}$ are the corresponding absolute frequencies at which $|Z|$ has the minimum and the maximum and G has the maximum value, respectively, for a given ionomer film modified QCM electrode.

ionomer-film modified QCM electrode in air (inset to Figure 4a), it is apparent that the hydration of the ionomer film dramatically modifies the operation of the quartz crystal. The θ-plot for the dry ionomer-film modified electrode in air (inset to Figure 4a) is for the thickest film (920 nm) studied and is representative of the series of modified electrodes with dry ionomer films of varying thicknesses in air. The QCM electrodes modified with dry ionomer thin films conform to

dx.doi.org/10.1021/ja4117457 | J. Am. Chem. Soc. 2014, 136, 5309−5322

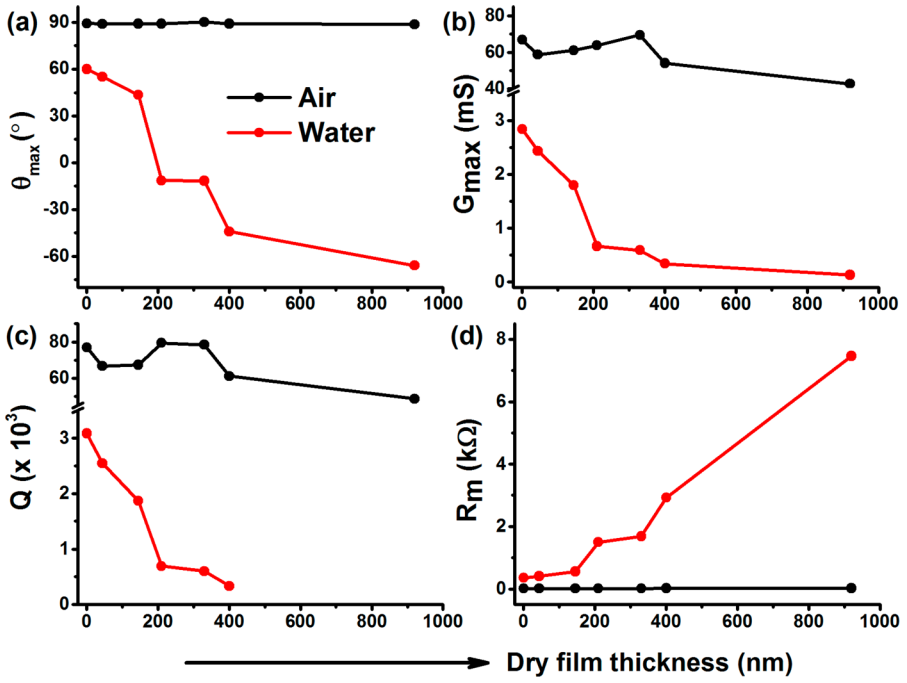

Figure 5. (a) θ_{max}, (b) G_{max}, (c) Q, and (d) R_m versus the dry thickness of the ionomer films (in the CO_3^{2-} form). Experimental parameters are the same as in Figure 4. The legend for (a) is applicable for the rest of the figure. The value of Q for the 920 nm thick film is not computed (see text).

the θ-response typical of a rigid film. The phase angle θ is $\sim -90°$ at frequencies far away from resonance, indicating the capacitive nature of the total impedance measured (refer to BVD model, Figure 3b). At the series ($\Delta f \approx -5$ kHz) and the parallel resonances ($\Delta f \approx 5$ kHz), $\theta = 0°$ as required by the resonance condition. Between the series and the parallel resonance frequencies, $\theta \approx 90°$ as the inductive load dominates the network impedance.

For the ionomer thin films in water, the θ-response is modified significantly (Figure 4a). θ_{max}, the maximum value of θ, is significantly less than 90° and decreases with increasing film thickness. The trend can also be followed by looking at Figure 5a. It should be pointed out that the liquid operation of the QCM will invariably result in a lower θ_{max} due to the viscous loading of the liquid. This is evident from the θ-plot of the bare QCM electrode in water. The presence of the hydrated ionomer film introduces an additional viscoelastic loading due to the swelling of the ionomer film in water. This viscoelastic loading will add resistive and capacitive loads to the network that will further reduce θ_{max}. The decrease in θ_{max} will be accentuated with increases in the film thickness due to the increased viscoelasticity of thicker films. Above a critical film thickness, ca. 200 nm, θ_{max} has a negative value implying that films much thicker than 200 nm will not be able to achieve a resonance condition. This observation is consistent with the results from the admittance plots (Figure 6) discussed later (vide infra).

Another interesting trend in the θ-plots for the modified electrodes in water is the change in peak profile with film thickness. Compared to the stepped profile of the θ-plots for the modified electrodes in air, the θ-plots for the modified electrodes in water have a peaked appearance. Also to be noted is the fact that the width of the θ-peaks (FWHM ~20−50 kHz) for the modified electrodes in water is much larger than the width of the θ-plateau (~10 kHz) for the modified electrodes in air. Both these trends are related to the increased energy

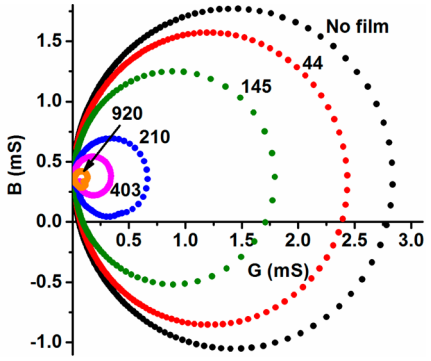

Figure 6. Admittance plots for the series of ionomer-film modified QCM electrodes in water shown in Figure 4. The dry thickness, in nm, of the ionomer film (in the CO_3^{2-} form) is specified by the number near the corresponding admittance locus. Experimental parameters are the same as in Figure 4

losses in the QCM or, equivalently, a decrease in the quality factor (Q) of the QCM (vide infra) in water vis-à-vis air (Figure 5c) because of its operation in a viscoelastic environment imposed by the hydrated ionomer film. Briefly, the absence of steps and the broadness of the peaks in θ-plots in water indicate that the resonance is not "sharp" due to the viscoelastic losses in the system. Finally, in case of severe viscoelastic loading, as in the case of the 920 nm film, there is splitting of the main peak and additional peaks appear at higher frequencies, indicating a complicated impedance response of the resonator. The origin of these extra peaks is not clear at present.

The G-plots (Figure 4b) are highly diagnostic of the operational efficiency of a composite QCM resonator. The height of the conductance peak (G_{max}) is inversely proportional to the motional resistance R_m (BVD model, Figure 3b); hence, it can be used to quantify the viscoelastic losses during QCM operation introduced by the hydrated ionomer film. The FWHM of the conductance peak is known as the *bandwidth*

dx.doi.org/10.1021/ja4117457 | J. Am. Chem. Soc. 2014, 136, 5309−5322

and is inversely proportional to the quality factor Q ($\approx f_{G_{max}}$/bandwidth), which is a measure of the QCM operational efficiency.[22] The trends can also be followed using Figure 5b–d. The composite resonators operating in air display close to ideal behavior. Their operation is characterized by high G_{max} values (~60 mS), narrow bandwidth (~75 Hz), high Q values (~70 000), and low R_m (~18 Ω). Importantly, these quantities do not vary greatly with film thickness. It is clear that, in the dry state, the ionomer thin films behave as rigid films and do not exhibit viscoelastic effects over the range of thicknesses studied.

As with the θ-responses, discussed earlier, hydration of ionomer films noticeably modified the conductance peak (Figure 4b) from that of the dry film (the right-hand-side inset to Figure 4b). The peaks are significantly smaller (lower G_{max}) and broader (higher bandwidth) when ionomer films are hydrated. This is clearly the manifestation of the viscoelastic losses arising from the solvent swelling of the films. It is also apparent, from Figure 5, that there is a discernible trend in the quantities of G_{max}, Q, and R_m with changing film thickness. Indeed, even without the film, the aqueous environment does affect these quantities as shown by the values for the case of the bare QCM electrode ($G_{max} \sim 3$ mS, bandwidth ~ 1600 Hz, $Q \sim 3000$, $R_m \sim 350$ Ω) due to viscous loading of the crystal by the liquid. However, additionally, the presence of the hydrated ionomer film dramatically affects the QCM performance parameters. G_{max} and Q decrease while R_m and the bandwidth increase with increasing film thickness. This is clearly as a result of the increasing viscoelastic losses in the hydrated films with increasing film thickness. For instance, the values of Q and R_m for the QCM electrode modified with a 403 nm thick ionomer film in water change by almost an order of magnitude compared to the values of the bare QCM electrode. Note that the value of Q is not computed for the 920 nm film in water because of the splitting of the conductance peak.

The admittance plots (G vs B) in Figure 6 conveniently summarize the effects of the hydrated ionomer thin films on the operation of the QCM in an aqueous environment. Two aspects of the admittance plots are worth highlighting. First is the radius of the circular trajectory, which is inversely proportional to R_m. Second is the crossing of the x-axis by the trajectory, which ensures that the composite resonator can achieve resonance at a particular frequency. Thus, admittance plots can be employed to easily diagnose viscoelastic effects in and operational failures of composite resonators. From the admittance loci in Figure 6, it is seen that the radius of the admittance locus decreases with increasing film thickness. This demonstrates that an increase in the swelling of the film with increasing thickness results in an increase in the viscoelastic losses, which is seen as an increase in the motional resistance R_m of the composite resonator. Consistent with the results from the θ-plots (Figure 4a), it is seen that for crystals modified with films thicker than ca. 200 nm in water, the admittance loci do not cross the x-axis, meaning that resonance cannot be achieved for films thicker than 200 nm.

In addition to demonstrating and quantifying the viscoelastic effects of the hydrated ionomer thin films, the impedance analysis was useful in determining the range of ionomer-film thicknesses that can be studied using the EQCM technique. We conclude that the ionomer films of dry thickness greater than ca. 200 nm cannot be studied by EQCM. However, it should be pointed out that, experimentally, ionomer films up to approximately 350 nm in thickness can be studied using the QCM technique. This is because the SRS QCM 200 controller used for the QCM studies implements capacitance cancellation. Basically, a variable capacitor incorporated in the QCM oscillator circuit can be adjusted to effectively reduce the magnitude of the static capacitance C_0 (refer to BVD model in Figure 3b). This shifts the center of the admittance locus downward along the y-axis (Figure 6). In favorable cases, the locus can now cross the x-axis allowing the circuit to achieve resonance.

4.2. EQCM Study of Methanol Oxidation at Ionomer-Film Modified Electrodes. *4.2.1. Motivation.* The oxidation of methanol (eq 6) at the ionomer-film modified Pt QCM

$$CH_3OH + 8OH^- \rightarrow CO_3^{2-} + 6H_2O + 6e^- \quad (6)$$

electrode was utilized to generate CO_3^{2-} locally in the film and study the carbonation dynamics in the film following the strategy previously outlined (Figure 2a). Methanol was chosen as the source of carbonate since it is neutral and hence is not expected to interact electrostatically with the cationic film. Furthermore, being a liquid, its concentration in the aqueous solution can be readily varied, allowing control over the amount of CO_3^{2-} generated.

From an application standpoint, studying the effect of methanol oxidation on the ionomer film is important since methanol is a potential fuel for direct methanol fuel cells. It is particularly suited for alkaline fuel cells (AFCs) based on the reportedly faster kinetics of methanol oxidation in alkaline media vis-à-vis acidic media.[23−27] Furthermore, the extent of CH_3OH crossover is expected to be lower in AFCs, compared to analogous proton exchange membrane fuel cells, because of the favorable direction of the electro-osmotic drag in AFCs.[4,6] Unlike the case of H_2-O_2 AFCs, where the only source of carbonation is from traces of CO_2 present in the reactant feeds, in direct methanol fuel cells, the issue of carbonation is exacerbated since methanol is itself a source of CO_3^{2-} upon its oxidation. Hence, the current study can also shed light on the carbonation phenomenon in such a scenario.

Another aspect that seems to have been largely overlooked, likely because of the intense focus on the carbonation process in AAEMs, are the effects of anions other than CO_3^{2-} on the performance of the membrane. This is especially true when small organic molecules, such as CH_3OH[28−30] and C_2H_5OH,[31] are used as fuels since these molecules do not undergo complete oxidation to CO_2. Particularly, in case of methanol oxidation on Pt in alkaline media, $HCOO^-$ has been indicated as one of the main oxidation products (eq 7) at high potentials

$$CH_3OH + 5OH^- \rightarrow HCOO^- + 4H_2O + 4e^- \quad (7)$$

(>0.6 V vs RHE).[28,29] Hence, investigating the effect of $HCOO^-$ on the membrane assumes significance in the context of methanol oxidation. We have attempted to address this point through the open-circuit QCM experiments discussed later in this paper.

4.2.2. Cyclic Voltammetric Studies. The cyclic voltammograms (CVs) obtained at the bare and the ionomer-film (210 ± 13 nm thick) modified Pt QCM electrodes with the simultaneous measurements of the changes in the resonant frequencies (Δf) and the motional resistances (ΔR_m) of the composite resonators are shown in Figure 7. Examining the CV for the bare electrode (Figure 7a.i), it is seen that CH_3OH

dx.doi.org/10.1021/ja4117457 | J. Am. Chem. Soc. 2014, 136, 5309−5322

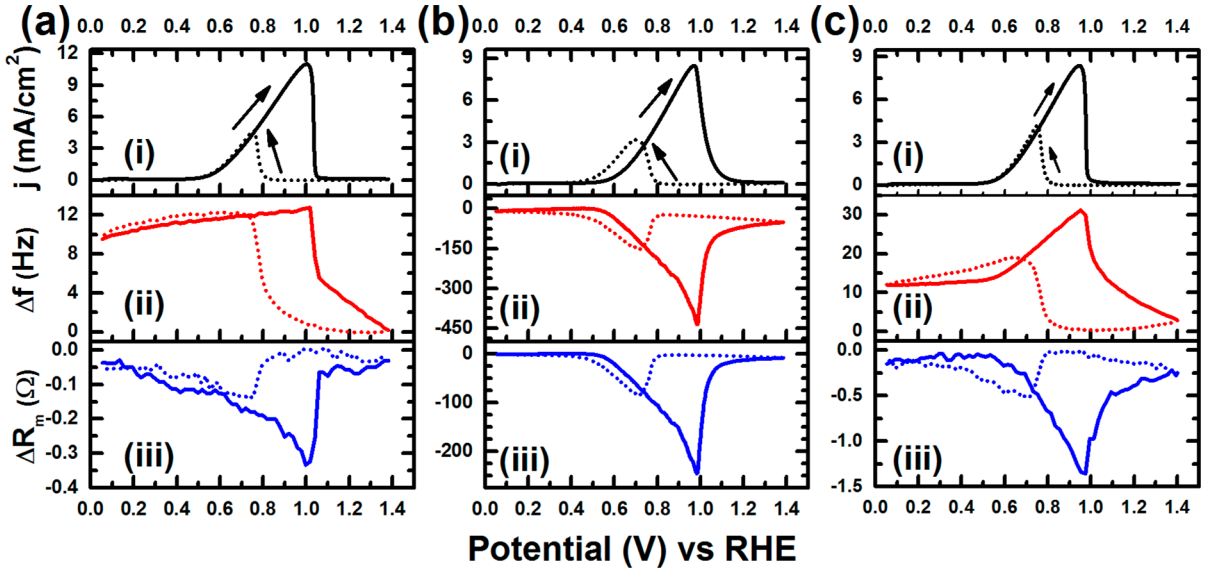

Figure 7. (i) Cyclic voltammetry with simultaneous (ii) frequency (Δf) and (iii) motional resistance (ΔR_m) change measurements in 0.1 M CH_3OH/0.1 M NaOH for (a) a bare Pt QCM electrode, (b) a Pt QCM electrode modified with an ionomer film of dry thickness, 210 ± 13 nm, and (c) a Pt QCM electrode modified with an ionomer film of dry thickness, 44 ± 13 nm. Scan rate: 20 mV/s. Solid line: forward scan. Broken line: reverse scan. Solution stirring rate: ~290 rpm.

oxidation on Pt starts at ~0.5 V, and there are two oxidation peaks, one in the positive-going scan and another in the negative-going scan with a lower peak current. It is also seen that the oxidation is inhibited at high potentials (>~1.0 V vs RHE) in the positive-going scan. This is due to the formation of a passivating oxide layer on the Pt electrode surface.[5] The onset of CH_3OH oxidation in the reverse scan (broken line) is shifted to more negative potentials, and the anodic peak current significantly lowered (~40%) compared to that in the forward (positive-going) sweep (solid line). This is suspected to be due to (1) the persistence of the inhibitory Pt−OH/oxide species formed at high potentials and (2) the inhibitory effect of OH^- adsorption.

The frequency changes (Δf) at the bare electrode during CH_3OH oxidation are dominated by the Pt-oxide formation/reduction processes (see Figure S1a in the Supporting Information). There is a slight increase in frequency during CH_3OH oxidation up until the onset of Pt-oxide formation (~1.0 V vs RHE). This frequency increase at the bare electrode is more pronounced in quiescent solution (see Figure S2 in the Supporting Information). The mass loss observed at low potentials (<1.0 V vs RHE) is suspected to be due to the oxidative removal of adsorbates (CO/CHO) derived from CH_3OH decomposition on the Pt surface.[5] Furthermore, this mass loss at the bare electrode is less prominent under active solution transport because of the rapid re-establishment of saturation coverage of adsorbates aided by the enhanced transport of CH_3OH to the surface. The Δf-plot (Figure 7a.ii) shows that the frequency decreases at high potentials (>~1.0 V vs RHE) corresponding to the formation of the Pt-oxide layer in the positive-going scan, and recovers in the negative-going scan because of the reduction of the oxide layer. As expected, the bare electrode does not exhibit any significant viscoelastic effects as indicated by the negligible changes in R_m during CH_3OH oxidation (Figure 7a.iii).

Satisfactorily, the presence of the ionomer film on the Pt electrode does not qualitatively affect the voltammetric response of the substrate either in the supporting electrolyte (see Figure S1b in the Supporting Information) or in the presence of CH_3OH (Figure 7b.i). However, it is interesting to note that the peak CH_3OH oxidation currents are lower (20−30%) at the ionomer-film modified electrode compared to the bare electrode. This is likely due to the shielding effect of the ionomer film on the Pt electrode. The changes occurring in the ionomer film during CH_3OH oxidation dramatically affect the crystal operation as demonstrated by the considerable changes in the frequency (Figure 7b.ii) and the motional resistance values (Figure 7b.iii) at the modified electrode vis-à-vis the bare electrode.

The frequency response of the modified electrode is noticeably different from that of the bare electrode. First of all, comparing the maximum frequency change ($|\Delta f_{max}|$: maximum value of $|\Delta f|$) during potential cycling, the $|\Delta f_{max}|$ for the modified electrode (210 nm thick ionomer film) is more than an order of magnitude higher (~430 Hz) than that of the bare electrode (~13 Hz). Second, unlike the case of the bare electrode, where Δf tracks mainly the formation and reduction of Pt-oxide layer, the Δf curve for the modified electrode mirrors the voltammetric profile of CH_3OH oxidation. The apparent mass increase observed at the modified electrode cannot be solely due to the Pt-oxide formation, but has to be due to a mass increase in the ionomer film. This is likely due to the incorporation of the anions (CO_3^{2-}/$HCOO^-$) generated during CH_3OH oxidation into the ionomer film. This conclusion is supported by the open-circuit QCM measurements described later in this paper (vide infra). There is a significant decrease in the R_m value during CH_3OH oxidation ($|\Delta R_m|$ (max) ~ 250 Ω) at the modified electrode, and just as in the case of Δf, ΔR_m strongly reflects the CH_3OH oxidation voltammetric profile. It is evident that the significant viscoelastic changes that the ionomer film undergoes are driven by the Faradaic processes at the electrode. In particular, since CH_3OH oxidation at the modified electrode is accompanied by a simultaneous decrease in both f and R_m, it is inferred that the incorporation of the electrochemically generated CO_3^{2-}/$HCOO^-$ in the film is accompanied by a deswelling of the

dx.doi.org/10.1021/ja4117457 | J. Am. Chem. Soc. 2014, 136, 5309−5322

film, most likely due to an egress of water molecules from the film. It is clear that the substantial viscoelastic effects exhibited by the ionomer-film during the oxidation of CH_3OH preclude any straightforward quantification (by the Sauerbrey equation) of the associated mass changes in the film. Hence, at the current stage of our research, we limit ourselves to a qualitative analysis of the EQCM results. Also, though partially addressed by the viscoelastic measurements presented in the present work, the extent and the role of water transport across the solution−film interface that should accompany the Faradaic process (CH_3OH oxidation) at the electrode and the subsequent ion-exchange in the film are important issues that warrant careful future investigations.

It is worthwhile to discuss the processes in the film that can potentially result in the significant changes in f and R_m observed at the film-modified electrodes. Focusing on the mass changes in the film during CH_3OH oxidation, one has to consider the mass fluxes at the two interfaces of the film, viz. the Pt-electrode/film and the film/solution interfaces. The consumption of OH^- during CH_3OH oxidation, as per eqs 6 and 7, leads to an overall excess of positive charge on the electrolyte side of the electrode/film interface. This excess charge needs to be screened by anions to ensure electroneutrality in the film. There are three possible sources of anions: (i) electrochemically generated $CO_3^{2-}/HCOO^-$ in the film, (ii) neutral ion-pairs ($Na^+ - OH^-$) in the film that can dissociate to produce free OH^- and (iii) solution OH^- transported into the film. Previous studies have suggested the application of a few general criteria (vide infra) in understanding the process by which electroneutrality is achieved in polyelectrolytes.[32,33] First, in responding to the instantaneous requirements of electroneutrality in films, the sources of charged species in the film will be exhausted first before using species in the solution. Second, the ejection of species from the film is more facile than ingress. On applying these guidelines to our results, it can be argued that, during CH_3OH oxidation, the electroneutrality in the ionomer film is most likely to be achieved immediately and primarily by (i) incorporation of the electrochemically generated $CO_3^{2-}/HCOO^-$ into the film and (ii) dissociation of neutral ion-pairs in the film necessarily followed by the expulsion of mobile cations (Na^+). Since the frequency change closely mirrors the Faradaic response of CH_3OH oxidation (Figure 7b), out of the two processes mentioned previously, the incorporation of the electrochemically generated $CO_3^{2-}/HCOO^-$ is strongly indicated to be the dominant method of achieving electroneutrality in the film. The transport of OH^- from the solution into the film may happen at longer times, but only if the species in the film are not able to ensure electroneutrality.

The decrease in R_m, during CH_3OH oxidation, indicates a deswelling of the film that has to be due to the egress of water from the film. This solvent exodus can be driven mainly by the two processes mentioned previously viz. (i) incorporation of $CO_3^{2-}/HCOO^-$ in the film and (ii) expulsion of mobile cations following the dissociation of neutral ion-pairs in the film. Open-circuit experiments discussed later indicate a very strong interaction of $CO_3^{2-}/HCOO^-$ with the film. If it is the case that $CO_3^{2-}/HCOO^-$ are strongly paired to the fixed cations in the film, then it is possible that these anions are not solvated to the same extent as OH^-, thus resulting in the loss of water molecules from the film. The exit of the solvated mobile cations could similarly contribute to the deswelling of the film.

In order to understand the effect of film thickness on the frequency and the viscoelastic changes observed for the modified electrodes, the above-described experiment was performed on a much thinner ionomer film (44 ± 13 nm) deposited on the Pt QCM electrode. The results are shown in Figure 7c. Compared to the thicker ionomer film studied previously (Figure 7b), the changes in f and R_m for the electrode modified with the thinner film are significantly smaller. Moreover, in contrast to the thicker film, the frequency increases slightly during CH_3OH oxidation for the thinner film (Figure 7c.ii) until the onset of Pt-oxide formation (~1.0 V vs RHE). In fact, a similar Δf profile is seen at the bare electrode in quiescent solution (see Figure S2 in the Supporting Information). It is likely that, since the forced convection in the solution will not be very effective in the film, the transport of CH_3OH to the electrode surface is hindered by the film. Hence, in the case of the thin film electrode, the adsorbates (CO/HCO) from CH_3OH are removed from the Pt surface at a faster rate than they are formed resulting in an overall mass loss. It is to be noted that, although viscoelastic changes of the thin film are small, the mass changes are now dominated by the Pt surface processes.

Since the number of fixed cations in the film is proportional to the film thickness, the amount of $CO_3^{2-}/HCOO^-$ incorporated into the film, and consequently the magnitude of frequency change at the modified electrode, will decrease with decreasing film thickness. For a sufficiently thin film, the frequency decrease (or the apparent mass increase), due to anion incorporation in the film, becomes small compared to even those associated with the electrochemical processes at the Pt electrode (both CH_3OH oxidation and Pt-surface processes). Hence, for sufficiently thin ionomer films, the mass changes at the modified electrode would be comparable to that of the bare electrode.

The viscoelastic effects observed for the thin ionomer film (Figure 7c) are also consistent with the above explanation. The ΔR_m profile for the thin film resembles that of the thicker film in that deswelling of the film is also observed during CH_3OH oxidation. However, the viscoelastic changes in the thin film are much smaller as evidenced by the much smaller magnitude of ΔR_m during oxidation vis-à-vis the thicker film (Figure 7b.ii). It should be pointed out that this effect was already anticipated from the acoustic impedance analysis of the ionomer films of varying thickness previously described.

The results discussed above for the thin ionomer film highlight the difficulty in quantifying the mass changes for the system of films studied by EQCM. The severe viscoelastic effects preclude application of mass quantification by the Sauerbrey relationship for thick films. Although the viscoelastic effects are manageable for thin films, the Δf associated with mass changes in the film are still difficult to estimate as they become comparable to, or smaller than, the Δf due to the electrochemical processes at the substrate electrode.

4.2.3. Chronoamperometric Study. As mentioned in the Methodology section previously, the advantage of employing an electrochemical method to study anion exchange dynamics (Figure 2a) is that, during the experiment, the concentration of the various species of interest, the fuel (CH_3OH) and the anions (OH^-, CO_3^{2-} and $HCOO^-$), are only locally affected, i.e., at the electrode surface and in the ionomer film. The electrode processes result in negligible changes to the bulk solution concentrations of these species. This is a useful feature since it allows us to perturb the film from a given steady state,

dx.doi.org/10.1021/ja4117457 | J. Am. Chem. Soc. 2014, 136, 5309−5322

such as by the oxidation of CH_3OH at the modified electrode, and then removing the perturbation and monitoring how the film relaxes. With this strategy, not only can we study CO_3^{2-}/$HCOO^-$ incorporation in to the film by driving CH_3OH oxidation at the Pt electrode, but by arresting the oxidation we can also determine if and how CO_3^{2-}/$HCOO^-$ are exchanged out by OH^- in solution. Thus, by this method, the anion exchange process in the ionomer film can be studied in both directions. The straightforward way to implement this strategy is to perform an EQCM experiment in which a series of potential steps, each step of appropriate duration, are executed at the modified electrode between potentials at which there is oxidation of CH_3OH or not. The results from such an experiment are shown in Figure 8.

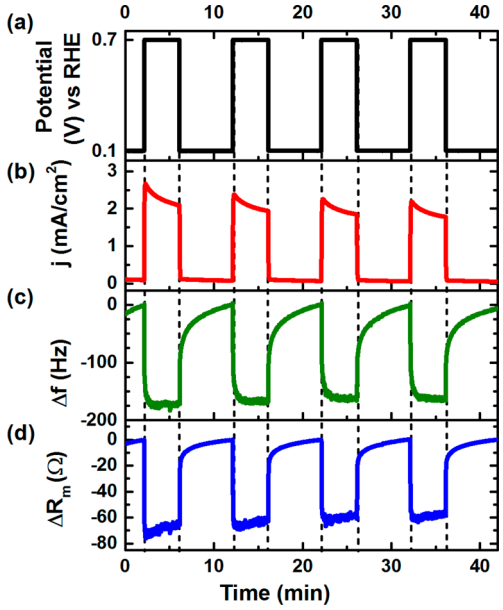

Figure 8. A series of (a) potential steps with (b) the corresponding current density obtained and the simultaneous (c) frequency (Δf) and (d) motional resistance (ΔR_m) changes measured at the ionomer-film modified Pt QCM electrode in 0.1 M CH_3OH/0.1 M NaOH. Dry film thickness: 210 ± 13 nm. Solution stirring rate: ~300 rpm.

Immediately after stepping the potential to +0.7 V vs RHE (Figure 8a), where the oxidation of CH_3OH takes place, a precipitous drop in the f (Figure 8c) and the R_m (Figure 8d) values of the modified QCM electrode was observed and, at longer times of the potential hold, the f and the R_m reached a more or less steady state value which was lower than that when there was no oxidation. This is consistent with the results from the cyclic voltammetric studies previously discussed (Figure 7b), where it was inferred that the decreases in the f and the R_m values during oxidation were due to the CO_3^{2-}/$HCOO^-$ incorporation in and a simultaneous deswelling of the ionomer film, respectively. Significantly, on stepping the potential back to +0.1 V where there is no oxidation, there is a slower recovery of the f and the R_m back to the originally higher values. We suspect that this apparent mass decrease and swelling of the film on arresting the oxidation are due to the slower exchange of CO_3^{2-}/$HCOO^-$ in the film by OH^- in the solution. It is significant that, on stopping the oxidation, the f and the R_m recover their preoxidation values since this means that the CO_3^{2-}/$HCOO^-$ uptake in the film is reversible. Similar potential step experiments carried out on the thin film electrode (44 nm thick film) yielded significantly smaller changes in f and R_m (see Figure S3 in the Supporting Information) compared to that for the thick film electrode. Besides, a mass loss was observed on driving CH_3OH oxidation at the modified electrode; similar to the case of the bare electrode. Clearly, as we noted previously, the mass changes at these thin film electrodes are dominated by the Pt surface processes.

It is interesting that CO_3^{2-}/$HCOO^-$ incorporation into the film is indicated to be faster than the displacement of CO_3^{2-}/$HCOO^-$ in the film by OH^- in the solution. This asymmetry in the anion-exchange process can be ascribed to a variety of factors. It could be that CO_3^{2-}/$HCOO^-$ interacts with the cationic sites in the ionomer film more strongly than OH^-. The results from the open-circuit QCM injection experiments, discussed later, do seem to support this hypothesis. The ionic transport constraints placed on the OH^- could also additionally contribute to the lower rate of exchange of CO_3^{2-}/$HCOO^-$ in the film by OH^-. Since CO_3^{2-}/$HCOO^-$ are generated right at the film–substrate–electrode interface, the displacement of OH^- in the film by the electrogenerated anions should be facile. However, for the reverse process, the OH^- ions need to be transported from the solution, partitioned at the solution–film interface, and then driven by diffusion and electromigration into the film to displace the CO_3^{2-}/$HCOO^-$. Such a discrepancy in the rates of exchange is also reminiscent of the "kinetic permselectivity" concept that was proposed to explain mass changes in redox polymer films where it was generally observed that the egress from the film of a species was more facile than the ingress.[33]

4.3. Open-Circuit QCM Experiments. *4.3.1. Motivation.* The results from the EQCM experiments in the preceding section have shown that the oxidation of CH_3OH at the modified electrode proceeds with an apparent mass increase in the film and is accompanied by its deswelling. Although it was suspected that these changes are due to the incorporation of the electrogenerated CO_3^{2-}/$HCOO^-$ into the film, as opposed to depletion of methanol, it was important to verify this hypothesis. Referring to eqs 6 and 7, we note that the oxidation of methanol at the modified electrode will affect the concentrations of CH_3OH, CO_3^{2-}, $HCOO^-$, OH^-, and H_2O in the film. We have attempted to understand, individually, the effects of changing concentrations of CH_3OH, CO_3^{2-}, and $HCOO^-$ in the film during CH_3OH oxidation by performing open-circuit QCM experiments following the strategy outlined previously (Figure 2b). This involved the addition of aliquots of concentrated solutions of the reactant (CH_3OH) or the products ($HCOO^-$/CO_3^{2-}) to the supporting electrolyte (0.1 M NaOH) in which the modified electrode is immersed and simultaneously monitoring the changes in f and R_m resulting from the change in the concentration of the species in the film. In this strategy, the concentration of a species in the film is imposed by changing its bulk solution concentration.

4.3.2. CH_3OH Addition. Increasing the concentration of CH_3OH in the solution over the range 0–0.1 M, and consequently, the concentration of CH_3OH in the film, results in a small but systematic increase in the frequency and a simultaneous decrease in R_m (Figure 9). The changes in the frequency and R_m with increasing concentrations of CH_3OH were nearly linear, with slopes of ~0.5 Hz/mM and ~25 mΩ/mM, respectively. However, these changes are far smaller than those observed during the CH_3OH oxidation at the modified electrode discussed previously (Figures 7 and 8). Hence, the

dx.doi.org/10.1021/ja4117457 | J. Am. Chem. Soc. 2014, 136, 5309–5322

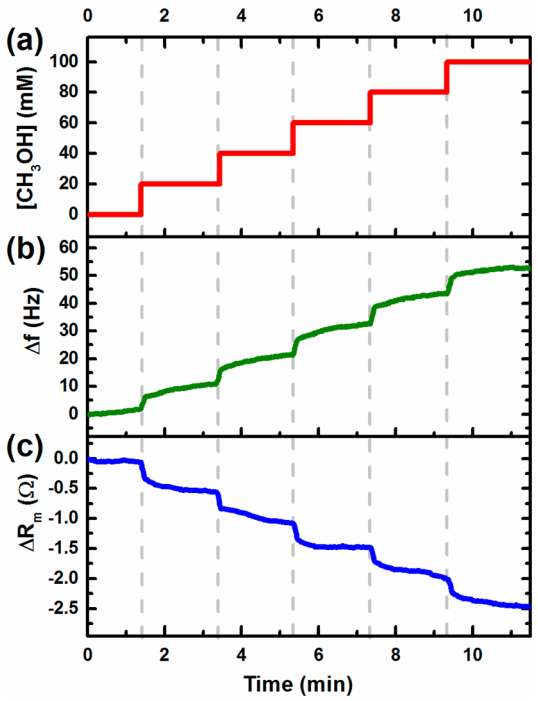

Figure 9. (a) Addition of aliquots of 3 M CH_3OH to 0.1 M NaOH in the EQCM cell in which a Pt QCM electrode coated with a 344 ± 10 nm ionomer film is immersed in the solution. (b) Δf and (c) ΔR_m versus time simultaneously measured. Initial volume of the solution (0.1 M NaOH) in the cell: ~90 mL. Each addition is an aliquot ~620 μL in volume added in ~5 s (at 7 mL/min) to a stirred solution (~300 rpm), resulting in a concentration increment of CH_3OH in the solution of ~20 mM per addition.

variation of the concentration of CH_3OH in the film during oxidation cannot explain the significant decreases in f and R_m observed in the EQCM experiments.

4.3.3. CO_3^{2-}/$HCOO^-$ Additions. The effects of the incorporation of the product anions of CH_3OH oxidation, CO_3^{2-} and $HCOO^-$, in the film was similarly studied by additions of concentrated aliquots of Na_2CO_3 and HCOONa, respectively. As is evident from Figure 10, the effects of CO_3^{2-} and $HCOO^-$ on the ionomer film are drastically greater in magnitude than that of CH_3OH. It is seen that the additions of CO_3^{2-}/$HCOO^-$ result in massive decreases in the frequency (Δf ~ 3−5 kHz) and the resistance parameter (ΔR_m ~ 350−600 Ω) of the modified electrode. This observation strongly suggests that the incorporation of CO_3^{2-}/$HCOO^-$ generated during CH_3OH oxidation into the film is directly responsible for the apparent mass increase in the film and the decrease in the viscoelasticity (swelling) of the film. Similar open-circuit experiments were conducted at bare Pt electrodes to gauge the contribution of the changes in the viscosity and the density of solution to the results obtained at the modified electrodes. The changes in f and R_m at the bare electrodes were found to be negligible (see Figure S4 in the Supporting Information) compared to those at the modified electrodes.

Besides serving to help understand the frequency and the motional resistance changes during CH_3OH oxidation at the modified electrode, the results of the CO_3^{2-}/$HCOO^-$ addition experiments also give us insights into the corresponding anion uptake processes in the ionomer film. This is most clearly seen in Figure 11 wherein we have constructed pseudoisotherms using the steady-state values of Δf (Figure 11a) and ΔR_m (Figure 11b) at each available solution concentration of the anion, X^{n-} (where X^{n-} can be either CO_3^{2-} or $HCOO^-$) obtained from Figure 10. The substantial uptake of CO_3^{2-}/$HCOO^-$ in the film signified by the large decreases in f suggests that both $CO_3^{2-}$and $HCOO^-$ strongly interact with the film; most likely with the cationic sites in the film. The observation that Δf reaches a saturation value at high concentrations of CO_3^{2-}/$HCOO^-$ is highly significant since it suggests that the uptake of CO_3^{2-}/$HCOO^-$ in the film is finite and controlled by

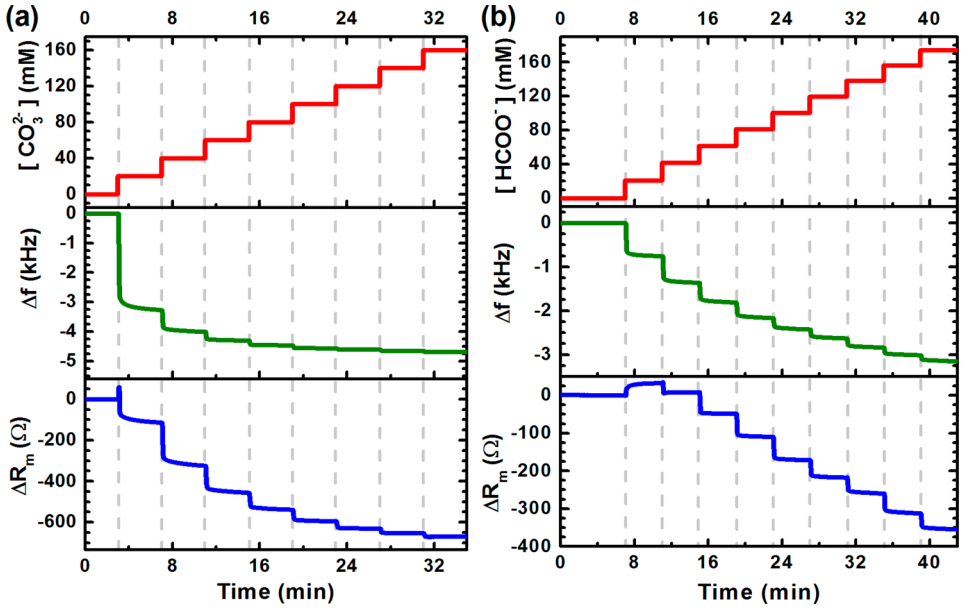

Figure 10. Δf and ΔR_m versus time during the addition of aliquots of (a) 2 M Na_2CO_3, (b) 2 M HCOONa to 0.1 M NaOH in the EQCM cell. A Pt QCM electrode coated with a 344 ± 10 nm ionomer film is immersed in the solution. Initial volume of the solution (0.1 M NaOH) in the cell: ~85 mL. Each addition is an aliquot ~900 μL in volume added in ~5s (at 10.8 mL/min) to a stirred solution (~300 rpm) resulting in a concentration increment of $HCOO^-$/CO_3^{2-} in the solution of approximately 20 mM.

dx.doi.org/10.1021/ja4117457 | J. Am. Chem. Soc. 2014, 136, 5309−5322

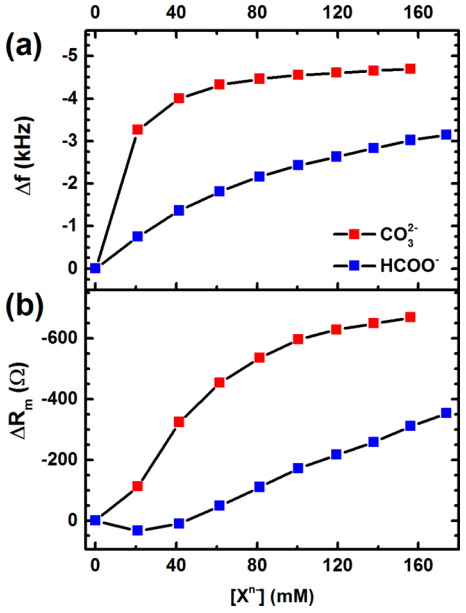

Figure 11. Plots of the steady-state values of (a) Δf and (b) ΔR_m versus the solution concentration of X^{n-} anion based on the data from Figure 10. X^{n-} is CO_3^{2-} or $HCOO^-$.

the film's ion exchange capacity. This is exactly what would be expected if there is no precipitation in the film. Hence, the present results validate the expected tolerance of AAEMs to carbonate precipitation.

The viscoelastic changes of the ionomer film indicated by the current set of R_m measurements and also from the previously discussed study of CH_3OH oxidation reveal an underlying phenomenon. It seems that the incorporation of CO_3^{2-}/$HCOO^-$ into the film results in its deswelling. Since typically swelling in polymer films is due to solvent uptake, this would suggest that the water content in the ionomer film is higher when it is in the OH^- form than when it is in the CO_3^{2-}/$HCOO^-$ form. Of course, in a sense, this is not surprising since the hydration spheres of CO_3^{2-}, $HCOO^-$, and OH^- will not be the same. In any case, it is apparent that the concomitant water transport in the film during the anion-exchange processes warrants careful study in the future.

Comparing the pseudoisotherms of CO_3^{2-} and $HCOO^-$, for a given anion concentration in the solution, CO_3^{2-} uptake in the film causes apparently higher mass and viscoelastic changes in the film when compared to $HCOO^-$. A higher partition coefficient for CO_3^{2-} anions is also indicated on the basis of the pseudoisotherm as the saturation CO_3^{2-} concentration in the film is reached at lower solution concentrations of CO_3^{2-} vis-à-vis $HCOO^-$. The results suggest that CO_3^{2-} might have a stronger interaction with cationic sites in the film compared to $HCOO^-$.

4.4. EQCM Study of Formate Oxidation at the Ionomer-Film Modified Electrode. The interplay between $HCOO^-$ and CO_3^{2-} in the film can be probed by studying the $HCOO^-$ oxidation at the ionomer film modified electrode. To this end, the ionomer film was spin coated on a Au QCM substrate sputter coated with a Pd thin film (~100 nm thick). The combination of a Pd thin layer electrode on a Au QCM substrate was chosen as Pd is highly active for $HCOO^-$ oxidation whereas Au is inactive.[34] A Pt QCM electrode was not employed since Pt is only weakly active for $HCOO^-$ oxidation.[35] It is to be noted that the deposited Pd thin film in contact with the Au QCM electrode still behaves as a rigid film during the QCM operation. Hence, any significant changes in R_m at the ionomer film modified electrode will be due to the changes in the viscoelasticity of the ionomer film.

Similar to the study of CH_3OH oxidation at the modified electrode discussed previously, both cyclic voltammetric and potential step experiments were conducted. The results from both sets of experiments are shown in Figure 12 and are consistent with each other. Focusing on the cyclic voltammetric

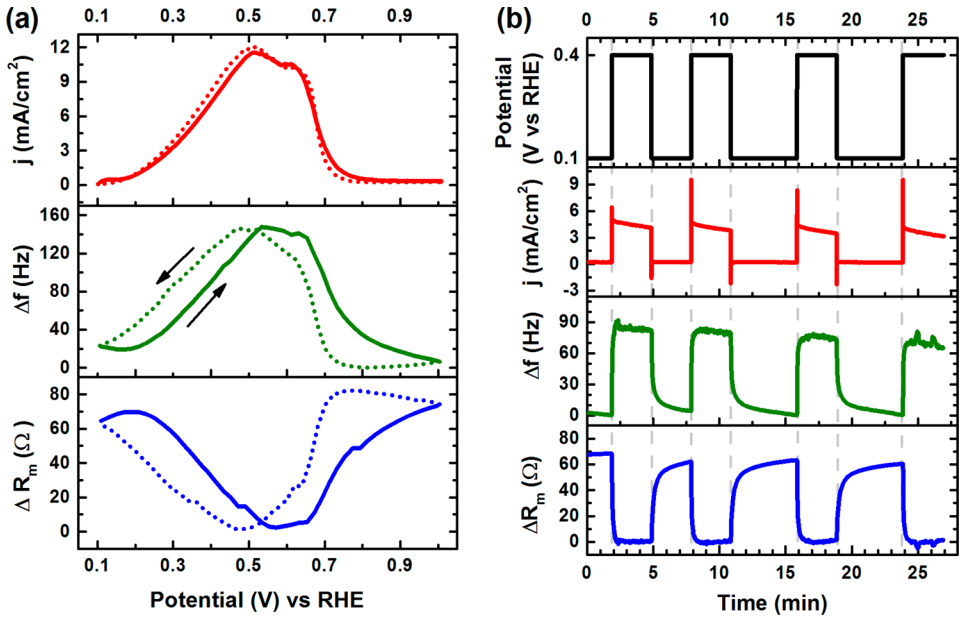

Figure 12. (a) Cyclic voltammetry and (b) potential step experiments with simultaneous frequency (Δf) and motional resistance (ΔR_m) change measurement in 50 mM HCOONa/0.5 M NaOH for a 326 ± 10 nm (dry thickness) ionomer-film modified sputter deposited Pd (~100 nm) on Au QCM electrode. Solution stirring rate: ~210 rpm. For (a), scan rate: 20 mV/s. In (a), the solid line and the broken line indicate the forward and the reverse scan, respectively.

dx.doi.org/10.1021/ja4117457 | J. Am. Chem. Soc. 2014, 136, 5309−5322

study (Figure 12a), the overall Δf and ΔR_m values for $HCOO^-$ oxidation at the ionomer film modified electrode are substantially higher than the corresponding values observed at the ionomer-film modified electrode in the absence of $HCOO^-$ (see Figure S5a in the Supporting Information) and at the bare Pd–Au composite QCM electrode in the presence of $HCOO^-$ (see Figure S5b in the Supporting Information). This implies that the apparent mass and the viscoelastic changes are due to the film processes driven by the $HCOO^-$ oxidation at the electrode.

During oxidation, it is seen that there is an apparent mass decrease in the film. This could be due to the displacement of $HCOO^-$ in the film by CO_3^{2-} generated during $HCOO^-$ oxidation (eq 8). From the results of the open-circuit QCM

$$HCOO^- + 3OH^- \rightarrow CO_3^{2-} + 2H_2O + 2e^- \quad (8)$$

experiments discussed previously (Figure 10), it was already inferred that both $HCOO^-$ and CO_3^{2-} can easily displace OH^- from the film. Moreover, on the basis of the pseudoisotherms (Figure 11), the ionomer films seem to have a stronger affinity for CO_3^{2-} than $HCOO^-$, meaning that the exchange of $HCOO^-$ in the film by CO_3^{2-} should be a favored process. On the basis of these arguments, the apparent mass decrease in the film during oxidation can be understood. It is postulated that the dominant process could be the insertion of doubly charged CO_3^{2-} anions that will result in the expulsion of two $HCOO^-$ anions per CO_3^{2-} inserted to maintain electroneutrality in the film. The overall apparent mass change (including any accompanying solvent transfer) during this process is postulated to be negative and consequently registered as a frequency increase during the oxidation. In a similar vein, the decrease in R_m during oxidation can also be explained by the same process. It is seen from Figure 11 that the magnitude of ΔR_m, on average, is 2–4 times higher for CO_3^{2-} compared to $HCOO^-$ for the same concentration of the anions in the solution.

4.5. Summary and Conclusions. Ex situ acoustic impedance studies demonstrated that the ionomer thin films exhibited significant swelling in water. The solvent plasticization of the polymer film increases in magnitude with an increase in film thickness. In order to validate the tolerance of the ionomer material to carbonate precipitation, a strategy involving the use of QCM technique to monitor the mass changes due to carbonate uptake in the film, either electrochemically or otherwise, was devised. In order to probe the dynamics of carbonation, in particular, and anion incorporation in the ionomer film, in general, EQCM experiments were carried out to monitor the mass changes in the film deposited on QCM electrodes in situ while relevant electrochemical reactions were driven at the electrode to generate anions that partition into the film.

The existence of severe viscoelastic effects in the ionomer thin films limited the quantitation of the mass changes in the film by the QCM technique. However, at the same time, the measurement of the motional resistance parameter allowed the changes in the film viscoelasticity to be monitored simultaneously with mass changes. This afforded critical insights into the dynamic rheological changes in the polymer that were accompanying the anion insertion/deinsertion processes.

In the EQCM studies, the oxidation of CH_3OH at the ionomer film-modified Pt QCM electrode was employed to generate anions, viz. CO_3^{2-} and $HCOO^-$, to understand the dynamics of anion exchange in the ionomer film. The oxidation of CH_3OH was found to proceed with an apparent mass increase and a decrease in swelling of the film. The CO_3^{2-}/$HCOO^-$ uptake in the film was found to be reversible in that arresting the production of the anions resulted in the apparent mass and the viscoelastic changes being reversed with time. Open circuit QCM experiments were also carried out wherein the solution concentration of CH_3OH, $HCOO^-$ or CO_3^{2-} was changed systematically to establish the effects each of these species, involved in CH_3OH oxidation, had on the mass and the viscoelastic changes in the ionomer thin film. CH_3OH was found not to influence the mass or the viscoelastic changes in the film significantly. However, the insertion of $HCOO^-$ and CO_3^{2-} into the ionomer film was observed to proceed with substantial increase in the apparent mass and a decrease in the swelling of the film. Importantly, the ionomer films were found to reach a saturation uptake of anions with an increase in the solution concentration of the anions, thus validating the tolerance of AAEM toward precipitation of salts within the polymer matrix. Interestingly, CO_3^{2-} is indicated to have a higher partition coefficient than $HCOO^-$, which suggests a stronger interaction between CO_3^{2-} and the polymer.

In an effort to further separate out the dynamics of $HCOO^-$ and CO_3^{2-} insertion in the film, the oxidation of $HCOO^-$ was carried out at the ionomer film-modified QCM electrodes. $HCOO^-$ oxidation was found to proceed with an apparent mass decrease in the film, which may be attributed to the replacement of every two $HCOO^-$ anions in the film by a doubly charged CO_3^{2-} anion. On analyzing the viscoelastic changes observed from all the experiments performed, a ubiquitous phenomenon was revealed, viz. the insertion of $HCOO^-/CO_3^{2-}$ into the ionomer film or equivalently the displacement of OH^- in the film by $HCOO^-/CO_3^{2-}$ invariably results in the deswelling of the film. It is inferred that the ionomer film in the OH^- form is more swollen than when in the $HCOO^-/CO_3^{2-}$ form. The current work also provides us with an important direction that needs to be pursued in the future regarding the anion exchange dynamics in the ionomer film, namely, the water transport in the film that is most likely accompanying the anion exchange process.

■ ASSOCIATED CONTENT

Supporting Information

EQCM responses of (1) bare and ionomer-film modified electrodes in NaOH solution, (2) bare electrode during CH_3OH oxidation under different solution transport conditions, (3) ionomer-film (44 nm thick) modified electrode during a chronoamperometric experiment in CH_3OH/NaOH solution, and (4) ionomer-film modified Pd electrode in NaOH solution and bare Pd electrode in HCOONa/NaOH solution. QCM responses of bare Pt electrode during aliquot addition experiments at open circuit. This material is available free of charge via the Internet at http://pubs.acs.org.

■ AUTHOR INFORMATION

Corresponding Author

hda1@cornell.edu

Notes

The authors declare no competing financial interest.

■ ACKNOWLEDGMENTS

This material is based upon work supported as part of the Energy Materials Center at Cornell (EMC^2), an Energy Frontier Research Center funded by the U.S. Department of Energy, Office of Science, Office of Basic Energy Sciences under Award Number DE-SC0001086. This work made use of the Nanobiotechnology Center shared research facilities at Cornell. This work made use of the Cornell Center for Materials Research Shared Facilities, which are supported through the NSF MRSEC program (DMR-1120296).

■ REFERENCES

(1) Winter, M.; Brodd, R. J. *Chem. Rev.* **2004**, *104*, 4245−4270.
(2) Wagner, F. T.; Lakshmanan, B.; Mathias, M. F. *J. Phys. Chem. Lett.* **2010**, *1*, 2204−2219.
(3) Debe, M. K. *Nature* **2012**, *486*, 43−51.
(4) Varcoe, J. R.; Slade, R. C. T. *Fuel Cells* **2005**, *5*, 187−200.
(5) Spendelow, J. S.; Wieckowski, A. *Phys. Chem. Chem. Phys.* **2007**, *9*, 2654−2675.
(6) Yu, E. H.; Krewer, U.; Scott, K. *Energies* **2010**, *3*, 1499−1528.
(7) Couto, A.; Rincón, A.; Pérez, M. C.; Gutiérrez, C. *Electrochim. Acta* **2001**, *46*, 1285−1296.
(8) Kita, H.; Nakajima, H.; Hayashi, K. *J. Electroanal. Chem. Interfacial Electrochem.* **1985**, *190*, 141−156.
(9) Perry, M. L.; Fuller, T. F. *J. Electrochem. Soc.* **2002**, *149*, S59.
(10) McLean, G. F.; Niet, T.; Prince-Richard, S.; Djilali, N. *Int. J. Hydrogen Energy* **2002**, *27*, 507−526.
(11) Merle, G.; Wessling, M.; Nijmeijer, K. *J. Membr. Sci.* **2011**, *377*, 1−35.
(12) Couture, G.; Alaaeddine, A.; Boschet, F.; Ameduri, B. *Prog. Polym. Sci.* **2011**, *36*, 1521−1557.
(13) Haynes, W. M.; Lide, D. R.; Bruno, T. J. *CRC Handbook of Chemistry and Physics 2012−2013*; CRC Press: Boca Raton, FL, 2012.
(14) Wang, Y.-J.; Qiao, J.; Baker, R.; Zhang, J. *Chem. Soc. Rev.* **2013**, *42*, 5768−5787.
(15) Noonan, K. J. T.; Hugar, K. M.; Kostalik, H. A.; Lobkovsky, E. B.; Abruña, H. D.; Coates, G. W. *J. Am. Chem. Soc.* **2012**, *134*, 18161−18164.
(16) Robertson, N. J.; Kostalik, H. A.; Clark, T. J.; Mutolo, P. F.; Abruña, H. D.; Coates, G. W. *J. Am. Chem. Soc.* **2010**, *132*, 3400−3404.
(17) Kostalik, H. A.; Clark, T. J.; Robertson, N. J.; Mutolo, P. F.; Longo, J. M.; Abruña, H. D.; Coates, G. W. *Macromolecules* **2010**, *43*, 7147−7150.
(18) Hibbs, M. R.; Hickner, M. A.; Alam, T. M.; McIntyre, S. K.; Fujimoto, C. H.; Cornelius, C. J. *Chem. Mater.* **2008**, *20*, 2566−2573.
(19) Grew, K. N.; Chiu, W. K. S. *J. Electrochem. Soc.* **2010**, *157*, B327.
(20) Siroma, Z.; Watanabe, S.; Yasuda, K.; Fukuta, K.; Yanagi, H. *ECS Trans.* **2010**, *33*, 1935−1943.
(21) Pan, J.; Chen, C.; Zhuang, L.; Lu, J. *Acc. Chem. Res.* **2012**, *45*, 473−481.
(22) Buttry, D. A.; Ward, M. D. *Chem. Rev.* **1992**, *92*, 1355−1379.
(23) Petry, O. A.; Podlovchenko, B. I.; Frumkin, A. N.; Lal, H. *J. Electroanal. Chem.* **1965**, *10*, 253−269.
(24) Hao Yu, E.; Scott, K.; Reeve, R. W. *J. Electroanal. Chem.* **2003**, *547*, 17−24.
(25) Parsons, R.; VanderNoot, T. *J. Electroanal. Chem. Interfacial Electrochem.* **1988**, *257*, 9−45.
(26) Prabhuram, J.; Manoharan, R. *J. Power Sources* **1998**, *74*, 54−61.
(27) Tripković, A. V.; Popović, K. D.; Grgur, B. .; Blizanac, B.; Ross, P. N.; Marković, N. M. *Electrochim. Acta* **2002**, *47*, 3707−3714.
(28) Morallón, E.; Rodes, A.; Vázquez, J. L.; Pérez, J. M. *J. Electroanal. Chem.* **1995**, *391*, 149−157.
(29) Matsuoka, K.; Iriyama, Y.; Abe, T.; Matsuoka, M.; Ogumi, Z. *Electrochim. Acta* **2005**, *51*, 1085−1090.
(30) Christensen, P. A.; Linares-Moya, D. *J. Phys. Chem. C* **2010**, *114*, 1094−1101.
(31) López-Atalaya, M.; Morallón, E.; Cases, F.; Vázquez, J. L.; Pérez, J. M. *J. Power Sources* **1994**, *52*, 109−117.
(32) Bruckenstein, S.; Hillman, A. R.; Swann, M. J. *J. Electrochem. Soc.* **1990**, *137*, 1323.
(33) Hillman, A. R.; Loveday, D. C.; Bruckenstein, S.; Wilde, C. P. *J. Chem. Soc. Faraday Trans.* **1990**, *86*, 437.
(34) Nishimura, K.; Machida, K.; Enyo, M. *J. Electroanal. Chem. Interfacial Electrochem.* **1988**, *251*, 103−116.
(35) John, J.; Wang, H.; Rus, E. D.; Abruña, H. D. *J. Phys. Chem. C* **2012**, *116*, 5810−5820.

■ NOTE ADDED AFTER ASAP PUBLICATION

This paper was published before all of the corrections were received from the authors. The corrections have now been applied and the revised version was re-posted on March 26, 2014.